

Interaction of a vortex ring with a piston vortex

By J. J. ALLEN AND B. AUVITY†

Department of Mechanical and Aerospace Engineering, Princeton University,
Princeton, NJ 08540, USA

(Received 5 March 2001 and in revised form 28 February 2002)

Recent studies on vortex ring generation, e.g. Rosenfeld *et al.* (1998), have highlighted the subtle effect of generation geometry on the final properties of rings. Experimental generation of vortex rings often involves moving a piston through a tube, resulting in a vortex ring being generated at the tube exit. A generation geometry that has been cited as a standard consists of the tube exit mounted flush with a wall, with the piston stroke ending at the tube exit, Glezer (1988). We employ this geometry to investigate the effect of the vortex that forms in front of the advancing piston (*piston vortex*) on the primary vortex ring that is formed at the tube exit. It is shown that when the piston finishes its stroke flush with the wall, and hence forms an uninterrupted plane, the piston vortex is convected through the primary ring and then ingested into the primary vortex. The ingestion of the piston vortex results in an increased ring impulse and an altered trajectory, when compared to the case when the piston motion finishes inside the tube. As the Reynolds number of the experiments, based on the piston speed and piston diameter, is the order of 3000, transition to turbulence is observed during the self-induced translation phase of the ring motion. Compared to the case when the piston is stopped inside the tube, the vortex ring which has ingested the piston vortex transitions to turbulence at a significantly reduced distance from the orifice exit and suggests the transition map suggested by Glezer (1988) is under question. A secondary instability characterized by vorticity filaments with components in the axial and radial directions, is observed forming on the piston vortex. The structure of the instability appears to be similar to the streamwise vortex filaments that form in the braid regions of shear layers. This instability is subsequently ingested into the primary ring during the translation phase and may act to accelerate the growth of the Tsai–Widnall instability. It is suggested that the origin of the instability is Görtler in nature and the result of the unsteady wall jet nature of the boundary layer separating on the piston face.

1. Introduction

The dynamics of vortex rings is a subject that has long fascinated researchers in fluid dynamics. Experimental research in this field is undergoing something of a renaissance with the use of synthetic jets, which are essentially a stream of vortex rings, for flow control. Comprehensive reviews of the behaviour of vortex rings are provided by Shariff & Leonard (1992) and Lim & Nickels (1995). Experimental generation of vortex rings often involves moving a piston through a tube, resulting in a vortex ring being generated at the tube exit. The development of a vortex ring

† Present address: Laboratoire d'Etudes Aérodynamiques/Centre d'Etudes Aérodynamiques et Thermiques, 43, rue de l'Aérodrome, 86036 Poitiers Cedex, France.

typically passes through a number of stages, i.e. the formation phase, the laminar phase, the transitional phase and, finally, the turbulent phase. Lim & Nickels (1995) note that whether the ring passes through all four phases is dependent on the initial conditions during the formation phase. During the formation phase, the early transient development of a vortex has been described using similarity arguments, Pullin (1978). Experiments and computations have had varied success in identifying a period of self-similar behaviour, Didden (1979), Pullin & Perry (1980), Nitsche & Krasny (1994), James & Madnia (1996), Heeg & Riley (1997). The explanations for these results not following similarity theory have been in terms of a number of effects, ranging from the self-induced effect to secondary vorticity and viscous entrainment by the ring. Nitsche & Krasny (1994), using a vortex sheet model for the vortex ring formation process, were able to identify the important factors causing departure from similarity theory as being the self-induced effect of the ring and the absence of a downstream component in the starting flow used for the similarity prediction. Their computation showed the correct scaling rates for core location and strength, but their result for the absolute strength of the ring was higher than experiments. They attributed this to the absence of secondary vorticity in their calculations. For short non-dimensional stroke lengths L/D , where L is the distance moved by the piston and D is the piston diameter, the end of the formation phase is determined by the cessation of the piston motion. It corresponds to the point of transition from a growing vortex ring of increasing strength to where the ring begins to convect as a result of its self-induced velocity. This point is marked by a contraction of the ring to reach a stable diameter, see Didden (1979) and Gharib & Weigand (1998). Didden (1979) states that the final non-dimensional diameter of the vortex is a function solely of L/D . It is also slightly dependent on the geometry of the generator, Lim & Nickels (1995). For fixed L/D , the vortex trajectory, and hence the final ring diameter, are almost independent on the Reynolds number for a wide range of Reynolds number up to 70 000, see Maxworthy (1977), the Reynolds number being based on the piston speed and the piston diameter.

The cause of the diameter reduction is an open question. It has been suggested (Didden 1979; Sheffield 1977), that the contraction is partly due to the effect of the image vortex in the wall and partly due to the *stopping vortex*. When the piston is brought to an abrupt halt, the primary vortex induces a separation at the corner of the generation geometry resulting in the formation of a vortex. This stopping vortex has been observed in a range of studies, e.g. Pullin & Perry (1980) and Weigand & Gharib (1997). The significance of the effect of the stopping vortex on the trajectory of the primary vortex is also an open question. For example Didden (1979) believed its effect to be weak whereas Heeg & Riley (1997) believed its effect to be strong. James & Madnia (1996) studied the ring produced at a nozzle and an orifice. Their computations show a difference in the final ring diameter between the two generation apparatus, for a given L/D . They attributed this difference to the lack of a wall effect for the nozzle, as the stopping vortex was present in both cases. Another reason for this difference could be the ingestion into the ring of the secondary vorticity generated on the walls close to the orifice. Also, if the effects of image are important it would be expected that the nature of the generation geometry would be important. The magnitude of L/D plays an important role in determining the resulting motion. If $L/D \sim 0.1$ Sheffield (1977) showed that the effects of the vortex image and stopping vortex are strong relative to the self-induced effect, and the potential exists for the ring to propagate back into the tube. For L/D of the order 0.5–4.5, the ring will convect away from the orifice under its self-induced field. The vortex will not continue to grow

as a discrete structure for increasing L/D and eventually the flow transitions to a jet, as mentioned by Saffman (1978). A criterion for the maximum piston displacement in relation to the tube diameter that results in a discrete vortex has been proposed by Gharib, Rambod & Shariff (1998) as being $L/D \sim 3.6\text{--}4.5$. A physical argument for this limiting value of L/D was suggested as follows: “the apparatus is no longer able to deliver energy at a rate compatible with the requirement that a steady translating vortex ring have maximum energy with respect to impulse-preserving isovortical perturbations”. This result has provoked a considerable amount of interest and resulted in a number of publications examining formation numbers. Mohseni & Gharib (1998) equate the circulation, impulse and energy (the system invariants) provided to the ring during generation to the properties of a particular class of rings with finite cores described by Norbury (1973). This formulation leads to the important result that the final ring diameter is essentially a function of the impulse, kinetic energy and circulation delivered to the ring during the formation phase. This suggests that the effects of image and stopping vortex are small, in as much as generator effects act to modify these invariants and resultant vorticity distribution.

As the vortex convects away from the generating orifice, if the Reynolds number based on piston speed and diameter exceeds 600, then the potential exists for it to develop a wavy structure. This is a precursor to breakdown to turbulence. An inviscid model for the appearance of azimuthal waves on the ring is described by Widnall & Tsai (1977). The wavenumber of the most unstable waves was found to be independent of Reynolds number. Experiments, however, show a variation in the number of waves on a ring, e.g. Liess & Didden (1976). The reason for this was explained by Saffman (1978) who determined that the shape of the vorticity distribution within the core can affect the number of waves that are formed on the ring. Studies of the behaviour of transition to turbulent rings are relatively limited. Maxworthy (1974) observed the appearance of the Tsai–Widnall instability prior to breakdown. Glezer (1988) notes that the transition to turbulence is preceded by the formation of a secondary instability on the primary vortex which appears similar in form to the secondary instability on a plane mixing layer, e.g. Bernal & Roshko (1986). Glezer (1988) noted the existence of Kelvin–Helmholtz instabilities on the vortex sheet connecting the vortex core to the generation orifice. He suggested that the ingestion of these instabilities into the vortex ring may accelerate the onset of turbulence. Glezer & Coles (1990) argue that these structures have a significant global effect in terms of acting to entrain fluid into the ring. The photographs of Maxworthy (1974) also show evidence of Kelvin–Helmholtz instabilities on the shear layer at a Reynolds number, Re_D , based on piston speed and piston diameter of the order 10 000. Lim (1997) conducted detailed experiments to examine the interaction of the shear layer instability with the vortex core and concluded that ingestion of the shear layer instability hastened the transition to turbulence.

Glezer (1988) suggested a generation geometry that consists of a tube that exits into a plane wall, with the piston finishing flush with the wall at the end of the generation process, forming an uninterrupted plane. This geometry has the obvious effect of removing the singularity that exists at the orifice edge of the tube exit when the piston motion stops (stopping vortex). This experiment raises the interesting question as to what happens to the *piston vortex* that has formed in front of the advancing piston. Experiments of Tabaczynski, Hoult & Keck (1970), Hughes & Gerrard (1971) and Allen & Chong (2000) have shown that for a Reynolds number greater than 400, based on piston speed and diameter, a vortex forms in front of the piston as it advances through the cylinder. The mechanism for this vortex formation

is the removal of the boundary layer from the cylinder wall in front of the advancing piston. T. T. Lim (2000, private communication) and Cater, Soria & Lim (1998) suggest from preliminary flow visualization studies that for $L/D = 3$ there is an interaction between the primary ring and the piston vortex via vortex leapfrogging, with the effect of hastening a transition to turbulence. Allen, Auvity & Smits (2000) used dye visualization to show the interaction of the piston vortex and primary ring for $L/D = 2$ and their vorticity field measurements showed the presence of the piston vortex and its ingestion into the primary core.

Based on this short review, a number of questions need to be addressed when using a generation geometry of the form proposed by Glezer (1988).

What is the effect of the stopping vortex? Can it be quantified using similar generation conditions (the same non-dimensional stroke length and piston speed) but different stopping geometry, i.e. whether the piston stops flush with the wall or inside the tube?

What is the effect of the piston vortex on the primary ring and what is the nature of the interaction between them?

Does the interaction change the transition process of the ring? Does the piston vortex trigger any particular type of instability on the primary ring? Does the universal transition map of Glezer (1988) need re-examination?

2. Experimental apparatus

A schematic of the vortex ring generator is shown in figure 1(a). The diameter of the piston D is 50.8 mm and the lead screw drives the piston up to a maximum speed, U_p , equal to 66.3 mm s^{-1} . The orifice plate exits into a $100 \times 50 \times 50 \text{ cm}$ tank and the maximum piston stroke is $4D$. The piston is driven with one velocity characteristic in these experiments, shown in figure 1(b). The average velocity of the piston during its stroke is defined as

$$\bar{U}_p = 1/T \int_0^T U_p(t) dt$$

where T is the duration of the piston motion. The length of the slug ejected from the tube can be written as

$$L = \int_0^T U_p(t) dt = \bar{U}_p T,$$

which is also the piston stroke. If the velocity profile at the orifice exit is assumed to be uniform spatially, then an approximation for the circulation delivered to the ring during generation is

$$\Gamma = (1/2) \int_0^T U_p^2(t) dt.$$

This model for the ring circulation is often referred to as the ‘slug’ model, see Shariff & Leonard (1992) and Lim & Nickels (1995) for details. Glezer (1988) pointed out that although this model cannot accurately predict the total circulation in the flow, it can be used for comparing the relative circulation of vortex rings formed from the same generator. Didden (1979) showed that this model for the circulation underestimates the strength of the ring by as much as 25%. The reasons are related to the non-uniform (spatial) nature of the velocity profile at the orifice exit during ring production and the ingestion of secondary vorticity. A program factor, P , that can be introduced to describe the effect of time variation of the piston velocity is

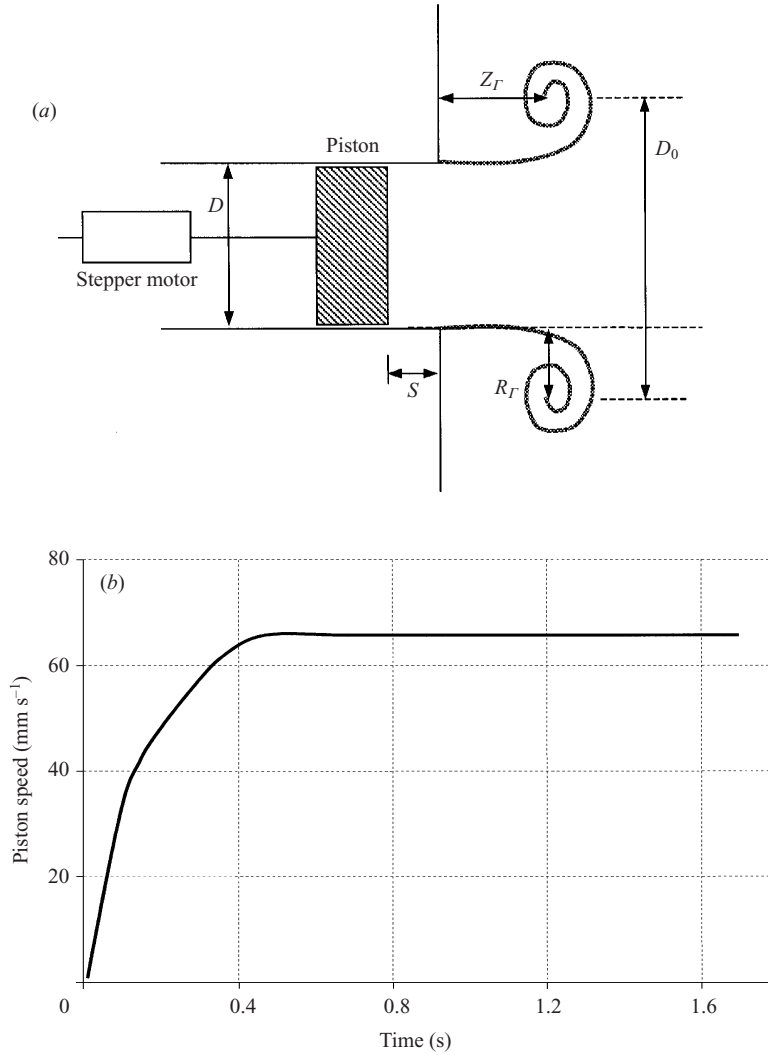


FIGURE 1. (a) Schematic of the experimental apparatus and (b) piston velocity characteristic.

expressed as

$$P = \int_0^1 U_p^2 / \bar{U}_p^2 d(t/T),$$

see Glezer (1988). Using this expression an approximation for the circulation of the ring is

$$\Gamma = PL^2/2T.$$

An invariant of the vortex motion is the impulse that is delivered to the fluid via non-conservative forces. The ring impulse, expressed in terms of the resulting vorticity field Ω , is

$$I = \frac{1}{2}\rho \int r \times \Omega dV,$$

where (z, r) represent cylindrical coordinates. Using the 'slug' model, the impulse

L/D	$U_p \text{ mm s}^{-1}$	$\bar{U}_p \text{ mm s}^{-1}$	P	Re_Γ
1.0	66.3	56.3	1.16	3317
2.0	66.3	61.8	1.06	6530
3.0	66.3	62.6	1.05	10 030
4.0	66.3	63.5	1.0	13 390

TABLE 1. Experimental conditions.

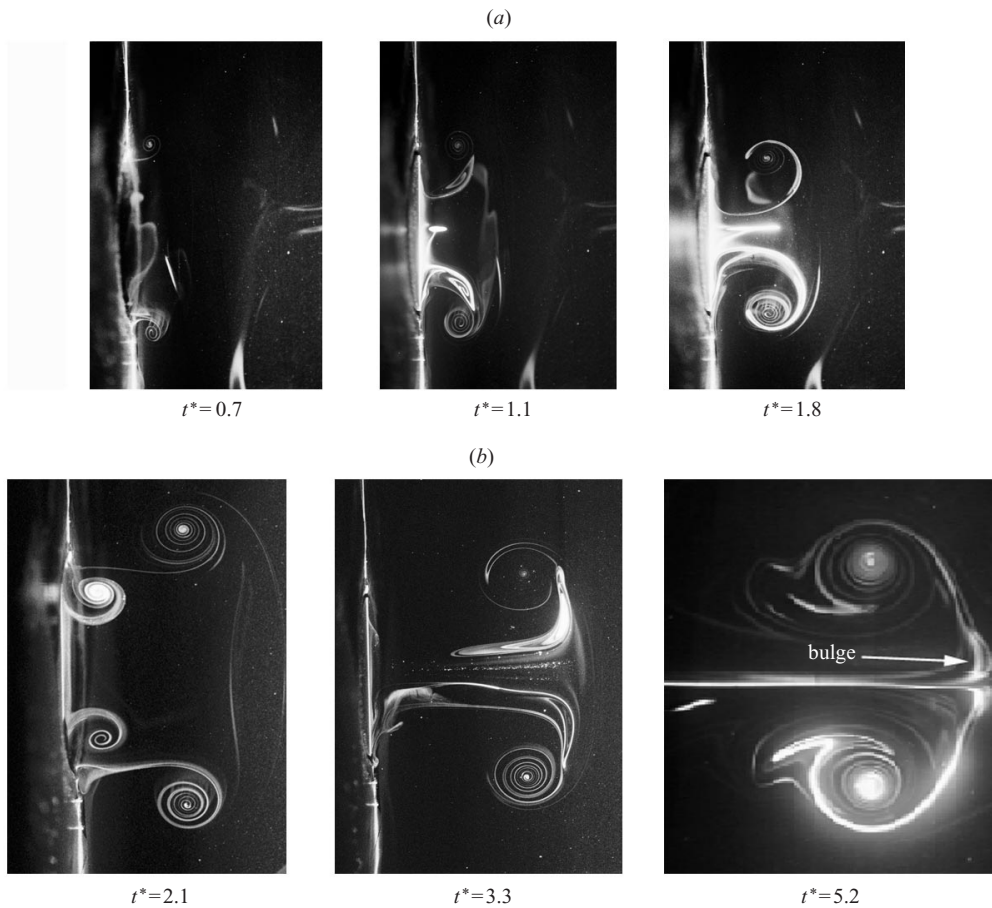


FIGURE 2(a, b). For caption see facing page.

delivered to the ring can be approximated as

$$I = \rho D^2 \frac{\pi}{4} \int_0^T U_p^2(t) dt = P \bar{U}_p L \rho \pi D^2 / 4.$$

This again involves the assumption that the velocity profile at the tube outlet is uniform and that the impulse of this uniform slug is all delivered to the ring. A Reynolds number that reflects the approximate impulse of the ring, from Glezer (1988), can be defined as

$$Re_\Gamma = P \bar{U}_p L / \nu = 2\Gamma / \nu.$$

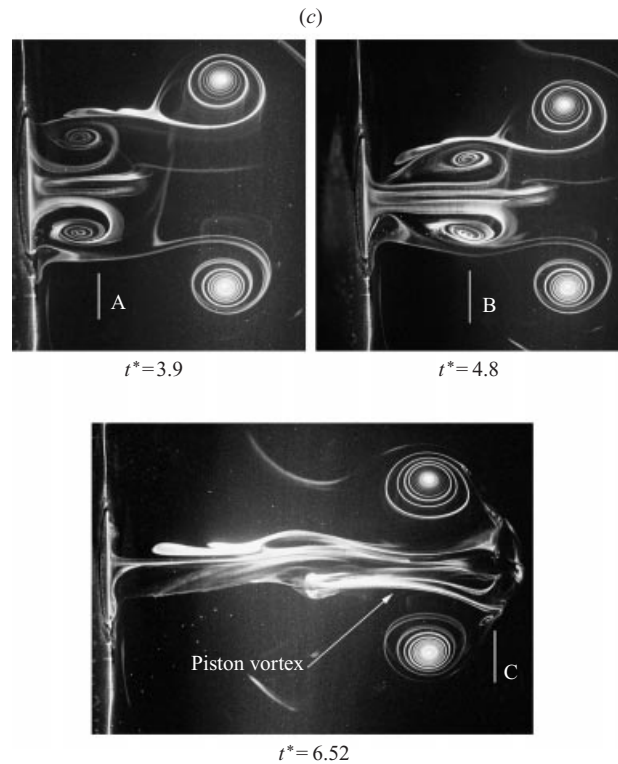


FIGURE 2 Piston vortex and vortex ring interaction for (a) $Re_F = 3317$, $L/D = 1$, (b) $Re_F = 6530$, $L/D = 2$, (c) $Re_F = 13390$, $L/D = 4$.

Details of the generation conditions for the current experiment are listed in table 1. A Reynolds number with length scale based on the piston diameter is Re_D .

3. Visualization of the interaction of the piston vortex with the primary ring

Fluorescent dye was introduced through the piston via diametrically opposite 0.5 mm holes, placed close to the piston/cylinder junction in order to visualize the piston vortex. Dye was also introduced through the tube at the junction of the tube with the wall to visualize the primary vortex. Laser cross-sections were taken in a plane through the axis of symmetry of the tube to record the interaction of the piston vortex with the primary ring. For the first set of flow visualization experiments, L/D was varied from 1 to 4 and the piston was stopped flush with the wall to determine over what range of L/D an interaction occurred. The images shown in figure 2 are of the piston finishing flush with the wall after moving a distance $L/D = 1, 2$ and 4 respectively. The non-dimensional time t^* shown in figure 2 is defined as $t^* = tU_p/D$; $t^* = 0$ corresponds to the start of piston motion.

In all cases the piston vortex is completely ingested into the primary ring. The flow visualization sequences in figure 2 show that the piston vortex convects rapidly through the core of the main ring toward the forward stagnation point of the primary ring as a result of the induction of the primary ring. When the piston vortex reaches the forward stagnation point it is rapidly stretched around the outside of the ring, see figure 2(b). Close to the forward stagnation point of the primary vortex some of the dye

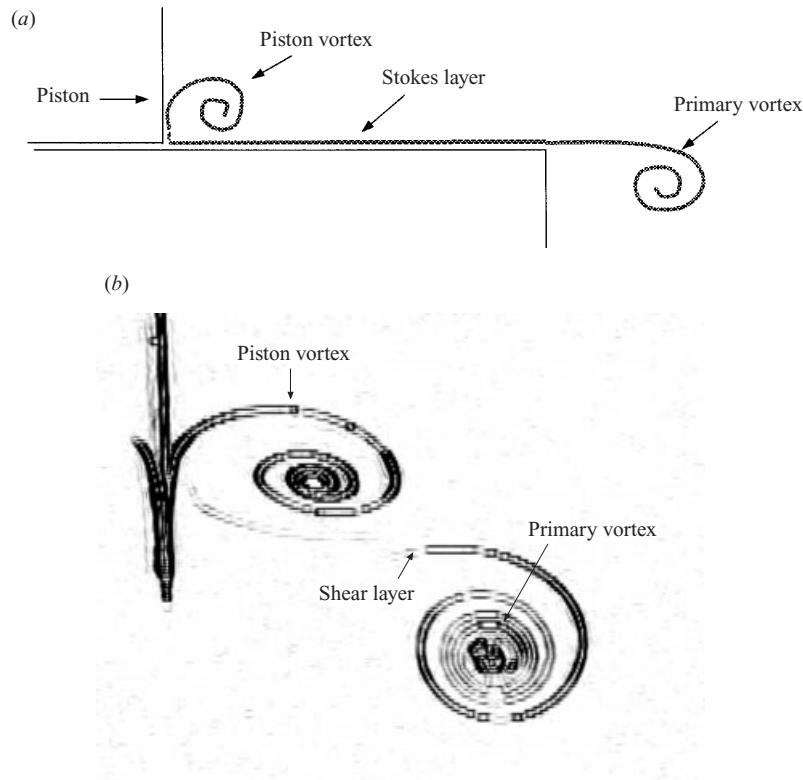


FIGURE 3. (a) Schematic of the relationship between piston vortex and primary vortex and (b) flow visualization experimental result for $Re_\Gamma = 6530$, $L/D = 2$, $t^* = 2.17$.

from the piston vortex appears to be drawn through the ring, forming a characteristic ‘bulge’ in front of the ring, figures 2(b) $t^* = 5.2$ and 2(c) $t^* = 6.52$. The photographs of Glezer (1988, figure 9(b) and 9(c)), show a bulging near the head of the primary ring. This feature in the current flow visualizations is a result of the ingestion of the piston vortex. When the piston was stopped inside the tube, no bulge was present.

The images in figure 2 show a distinctly tighter spiral shape for the primary ring core than the piston vortex. This would indicate the presence of stronger vorticity in the primary ring core than in the piston vortex (this result is confirmed by the particle image velocimetry (PIV) measurements presented in §6). Detailed PIV experiments of Allen & Chong (2000) have shown that the piston vortex circulation, $\Gamma_{Piston\ vortex}$, is of the order 22% of the ‘slug’ flow model of the primary vortex, i.e. $\Gamma_{Piston\ vortex}/\nu = 0.11Re_\Gamma$. This result is independent of D . In terms of vortex sheets, the piston vortex and primary vortex represent separate ends of a layer of vorticity. Connecting these two structures is the layer of vorticity (boundary layer) on the cylinder wall. As the piston progresses through the tube this layer is both ejected from the orifice (primary vortex) and scraped up in front of the advancing piston (piston vortex). The relationship between the two structures is shown schematically in figure 3(a). The connecting shear layer between the two structures is clearly evident in the photograph in figure 3(b), which shows the pair at the instant the piston motion has ceased and the piston vortex is being ejected from the tube.

Figure 4(a–c) shows visualizations of a section of the ring at large t^* , during the steady translation phase. In figures 4(a) and 4(b) the characteristic bulge leading the

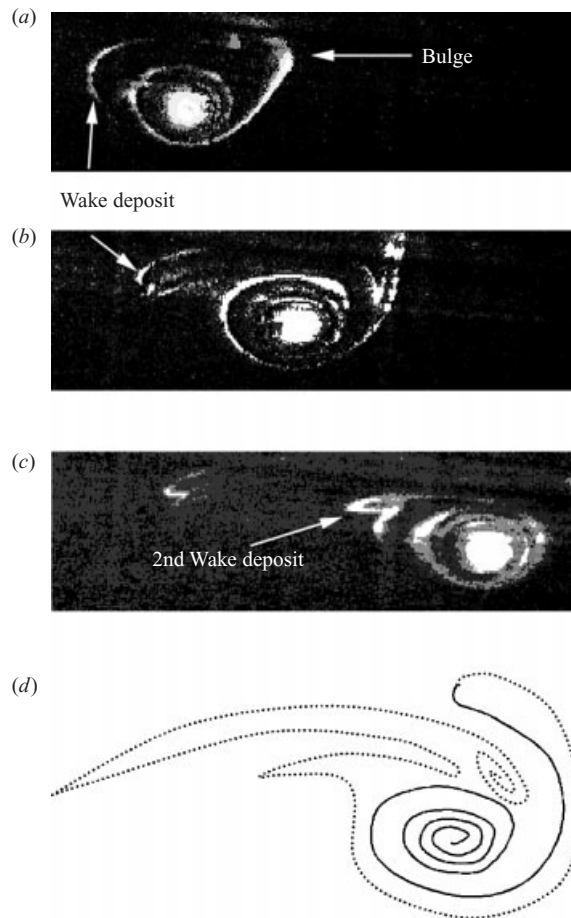


FIGURE 4. $Re_\Gamma = 10\,030$, $L/D = 3.0$: (a) $t^* = 6.5$, (b) $t^* = 7.8$, (c) $t^* = 10.3$. (d) Interpretation of vortex sheet folding.

ring can be seen along with the dye from the piston vortex being deposited into the ring wake. In figure 4(c) the bulge in figure 4(a) has been convected around the outside ring and a second discrete deposit of dye appears to have been made into the wake. The suggested folding and stretching pattern of the vortex sheets required to produce this detrainment is illustrated in figure 4(d). The darker line marks the vortex sheet consisting of the primary ring and shear layer, while the dotted line indicates the evolution and distortion of the piston vortex. This pulsing of the vortex ring would indicate that the streamline topology should show an unsteadiness and a mechanism for detrainment.

A recent computational paper by Nitsche (2001) suggests that the shedding of vorticity into the wake of the ring is related to the variational principle of Lord Kelvin which, for axisymmetric rings, means that the kinetic energy is at a local maximum, with respect to perturbations that preserve the circulation and impulse of the ring. Computational studies, e.g. Rom-Kedar, Leonard & Wiggins (1990) and Pozrikidis (1986), have shown how a perturbation to a vortex ring that is represented as an idealized symmetric vorticity distribution can result in unsteady entrainment and detrainment.

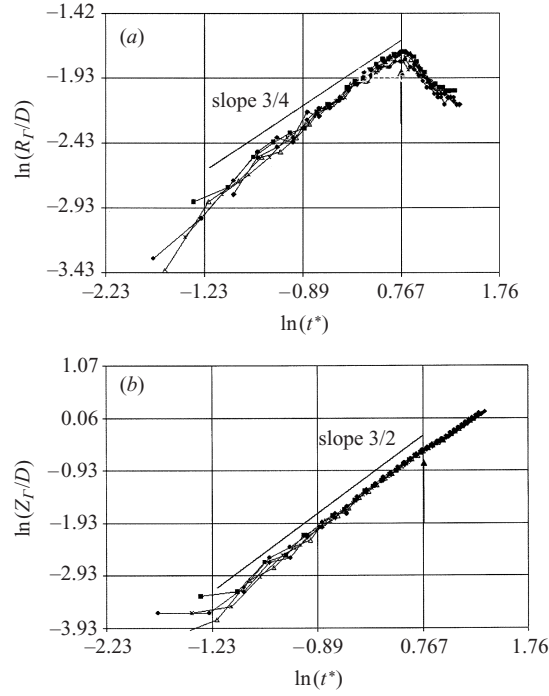


FIGURE 5. Variation of the primary ring core location, R_r and Z_r , with respect to time for $Re_r = 6530$.

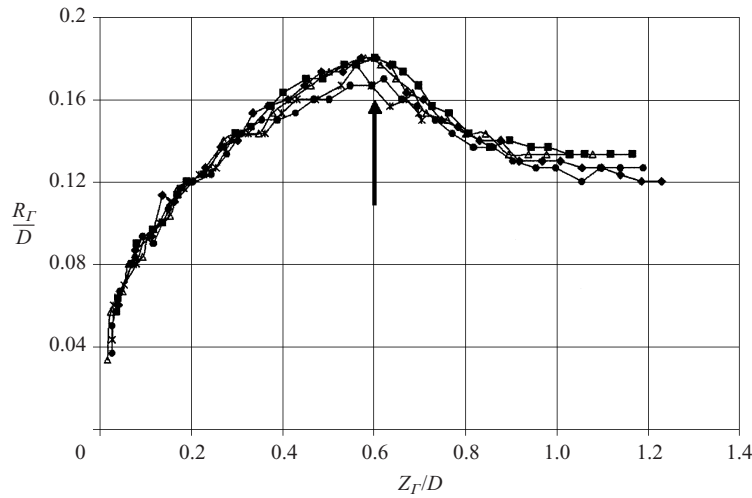
One obvious question that arises from these flow visualization results is what is the effect of varying the location where the piston motion is terminated, and at what S/D does the piston vortex/vortex ring interaction cease, where S is the distance from the tube orifice that the piston ceases its motion see figure 1(a). Flow visualization experiments for $L/D = 2.0$ and $Re_r = 6530$ revealed that any cessation of motion of the piston inside the tube reduces the amount of dye entrained from the piston vortex into the primary ring. The case $S/D \sim 0.3$ appeared to be the limit. When the piston ceases its motion inside the tube for $S/D > 0.3$ there is no ingestion of dye from the piston vortex.

4. Global effects

A strong interaction of the piston vortex with the primary ring may alter the primary ring vortex trajectory, compared to the case where the piston motion is stopped inside the tube. Vortex trajectories were therefore measured for the case of $L/D = 2$ and $Re_r = 6530$. The Reynolds number was selected to enable a comparison with the data sets of Didden (1979) and Weigand & Gharib (1997). The piston was stopped flush with the wall, or $2D$ inside the tube. Measurements were made of the position of the core of the primary vortex, (Z_r, R_r) , as defined in figure 1, using dye visualization.

4.1. Transient development and ring contraction

The initial phase of the ring development is defined as while the piston is in motion. Results for the trajectory of the vortex core during this period, and shortly after the motion ceases are shown in figures 5 and 6. The distinguishing aspect of these plots is

FIGURE 6. Trajectory of primary ring core for $Re_F = 6530$.

that the trajectories are essentially identical. The data set for the R_F coordinate shows a $t^{3/4}$ growth during the development phase, see Pullin (1978). The Z_F coordinate shows a considerably faster growth rate, typically $t^{3/2}$. These measurements of R_F and Z_F are similar to those of Didden (1979) and Weigand & Gharib (1997), who both used a tube as the exit geometry to generate vortex rings. The time at which the piston is stopped, $t^* = 2.17$, is identified by an arrows in figure 5 and 6. At this point the trajectory of the ring undergoes a rapid reduction in diameter, before convecting for a time with an approximately constant velocity. For a specific L/D Didden (1979) and Weigand & Gharib (1997) found an independence of core trajectory from piston velocity.

The interesting aspect of the data in figure 6 is the fact that the contraction is almost identical for the case when the piston is stopped inside the tube, and hence a stopping vortex is formed, and the case when the piston finishes flush and the piston vortex is ingested. The final ratio of vortex diameter D_0 to piston diameter is $D_0/D = 1.23$ which is in agreement with the empirical formulation of Auerbach (1987). This result suggests that the effect of the stopping vortex, produced at the orifice corner when the piston motion ceases, has little effect on the core trajectory and hence diameter. It would also seem to indicate that the effect of the piston vortex is weak.

The contraction of the ring diameter is also a feature of the studies where a 'nozzle' is used as the generation device, e.g. Didden (1979) and Weigand & Gharib (1997). These experiments, for $L/D = 2$, give a final vortex diameter of $D_{vortex}/D = 1.32$. The differing diameters for these two production devices can be also seen in the computational data of James & Madnia (1996). Note that this difference exists for the ring characteristics produced at a tube and orifice for the same piston speed and stroke length. Auerbach (1991) in a series of careful measurements notes for an orifice exit 60% of vortex fluid is tube fluid and 40% entrained fluid and for a tube exit 80% is tube fluid and 20% is entrained fluid.

The current literature on vortex rings has focused on the ring invariants, i.e. strength Γ , impulse I and kinetic energy T , and the way these invariants are delivered by the generation apparatus. Classification of the ring from its invariants stems from the

work of Norbury (1973) who proposed a class of vortex rings that were characterized by a vorticity distribution that was proportional to the distance from the axis of symmetry, $\omega = \Omega r$. Norbury rings are classified by a parameter α that represents the ratio of the area of the vortex to a length scale of the vortex. The range of α from 0 to $\sqrt{2}$ represents rings of small cross-section to Hill's spherical vortex. Each α yields a unique ring and associated invariants. These rings are somewhat idealized in that the vorticity distributions in experimental rings tend to be more Gaussian, but provide a useful framework in which to consider the behaviour of experimentally produced rings. The results of Norbury (1973) would seem to imply that the role of the image system and stopping vortex is not important in affecting the final diameter as it is defined by the invariants of production. They would also suggest that the rings produced at an orifice and nozzle, with the same L/D and velocity characteristic, are different as a result of how the apparatus delivers the invariants. Rosenfeld, Rambod & Gharib (1998) for example mention that the circulation of a ring produced at an orifice and nozzle can differ by as much as 5% and the suggested reason is a difference in vorticity cancellation. The computations of James & Madnia (1996) show a significant difference in the total impulse of the flow field for a ring produced at a nozzle and orifice. Unfortunately they do not calculate the impulse of the vortex alone for comparison.

Variations in the way the impulse is delivered to the rings for different geometries may be explained by considering the self-similar computations of Pullin (1978). In these two-dimensional calculations of the starting flow past a 90° wedge and a flat plate a clear difference exists in the location of the vortex core, for a given strength, and hence it can be inferred that there will be a difference in impulse. This is a direct result of the flow geometry and system of images used for both calculations. Hence in conclusion it is suggested that the ring contraction is not a direct result of the system of images and stopping vortex but rather the ring relaxing to its natural state, which is a function of its invariants. The generation geometry appears to be important in terms of determining how these invariants are produced.

4.2. Piston vortex leapfrogging

Figure 7(a) shows the Z_r coordinate of the ring for larger values of t^* for $L/D = 2$, $Re_r = 6530$, and the two stopping geometries being considered, $S/D = 0$ and 2. When the piston vortex is ingested, the velocity of the primary core slows at $t^* \sim 4.2$. This correlates with a deceleration of the ring and occurs as the piston vortex is being convected through the ring, as shown in figure 2(b), $t^* = 3.3$. The data shown for $S/D = 2$ display no such deceleration and the velocity of the ring appears to be almost constant. To more clearly illustrate the effect of the piston vortex as it orbits the primary ring, the mean Z_r core location was subtracted from the data sets. The results of this transformation are shown in figure 7(b). The mean location was based on the linear fit to the $S/D = 2$ data set in figure 7(a).

These results indicate the presence of a vorticity distribution of the form sketched in figure 8. This distribution would act initially to decelerate the primary ring while the piston vortex accelerates through the core in a form similar to vortex leapfrogging, e.g. Yamada & Matsui (1978). As the piston vortex is comparatively weak compared to the primary ring, the effect of the piston vortex and hence the deceleration of the ring is weak, while the effect of the ring on the piston vortex is strong.

The plots in figure 7(a, b) would also seem to indicate that at $t^* \sim 10$ for identical Re_r there is a clear difference in the convection speed. To clarify this, the time at which the primary core reached $Z/D = 7.3$ for $L/D = 2$ and $Re_r = 6530$ was

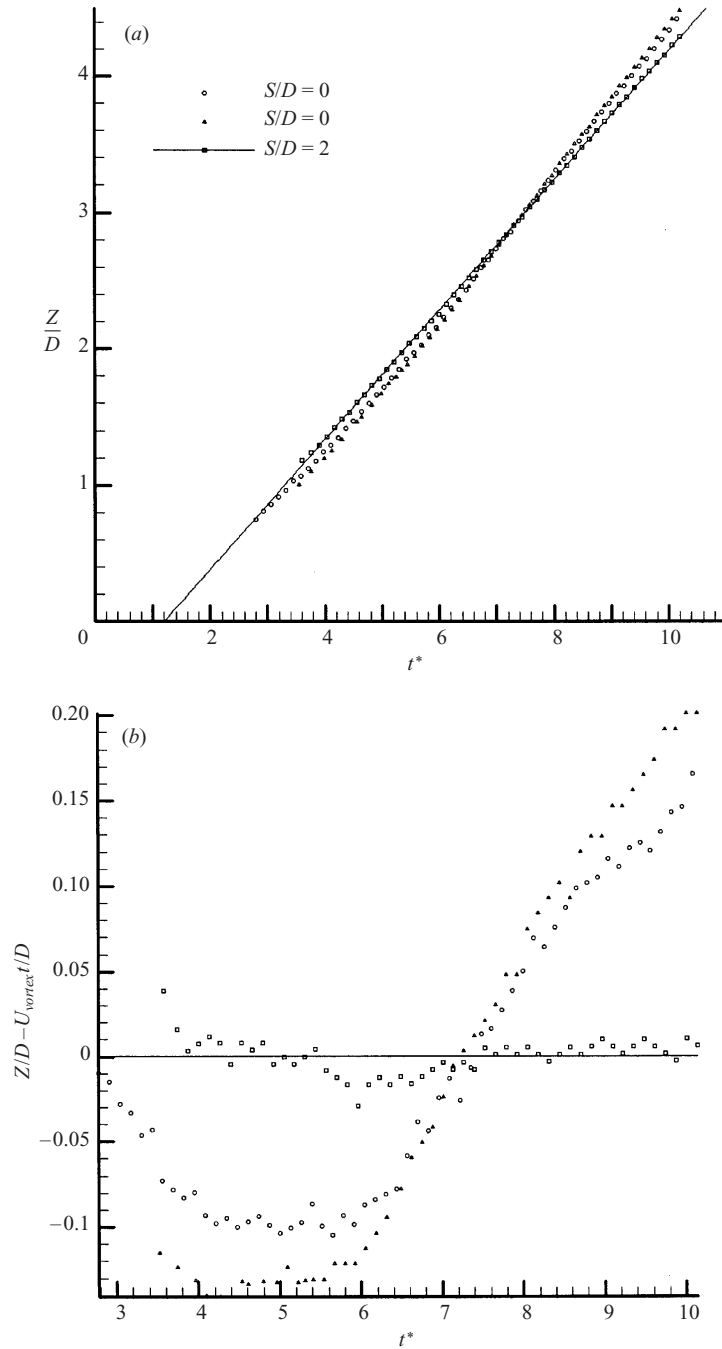


FIGURE 7. (a) Vortex core trajectories for $Re_T = 6530$, $L/D = 2$, $S/D = 0, 2$, and (b) vortex core trajectories with mean core location for $S/D = 2$ subtracted to illustrate leapfrogging of the $S/D = 0$ case.

measured, and was found to be $t^* = 15.1 \pm 0.1$ for the piston finishing flush with the wall and $t^* = 16.4 \pm 0.1$ for the case when the piston finished $2D$ inside the tube. The ring diameters were equal in both cases. Therefore the distance travelled by the rings for a given interval is different, indicating a difference in ring strength, which is a

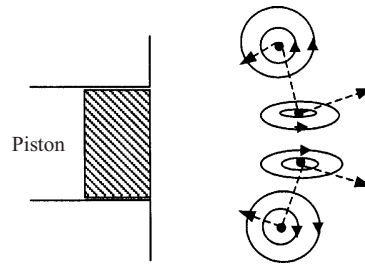


FIGURE 8. Leapfrogging and mutual induction effects of the primary ring and the piston vortex, resulting in a deceleration of the main ring.

direct consequence of ingestion of the piston vortex. To check this the location of the vortex core was measured for $Re_T = 10\,030$, $L/D = 3$, and $S/D = 0$ and 1. The data showed a significantly different terminal speed. The time to reach $Z/D = 5.02$ for the $S/D = 0$ case was $t^* = 11.3 \pm 0.1$ and for $S/D = 1$, $t^* = 12.3 \pm 0.1$. The conclusion that the rings have differing strengths and that a form of leapfrogging is occurring is confirmed by the PIV measurements, § 5.

The major source of error in these measurements is not resolving the location of the ring core, but cycle to cycle variations, caused by residual motions in the tank. For these experiments, the tank was allowed to settle for about 30 minutes between runs. If the settling time was not sufficient, misalignment of the rings occurred during ingestion, producing non-axisymmetric leapfrogging.

5. Topology of piston vortex/vortex ring interaction

PIV experiments were performed to generate quantitative velocity and vorticity information during the development phase. The data acquisition system consisted of an argon ion laser, an externally triggered Cohu 6600-3000 series full frame transfer video camera, 659×496 pixels, with 10 bit resolution, a General Scanning 6120DT series oscillating mirror and an Epix frame grabber. Details of the PIV system hardware and software, that are capable of producing a time difference between image of the order 0.5 ms are contained in Allen & Smits (2001) and Allen *et al.* (2000).

Figure 9 shows a sequence of streamline patterns for the case when the piston finishes flush with the wall and inside the tube with application of a bias velocity equal to the speed of the piston. From these streamline patterns the presence of the piston vortex is clearly evident. The piston vortex can be seen convecting through the primary vortex as in the dye visualizations. Vorticity fields were generated from the velocity data sets using a global spline technique, as outlined in Spedding & Rignot (1993). Figure 10 shows a sequence of the developing vorticity fields when the piston finishes flush with the tube exit. Non-dimensional vorticity is defined as $\omega = \Omega U_p/D$ and the vorticity contours in these plots are separated by three non-dimensional units.

Figure 10(a) shows the development of the primary ring while the piston vortex is still located inside the cylinder and the piston is still in motion. In figure 10(b) the piston vortex can be clearly seen emerging from the cylinder. This vorticity distribution appears very similar in form to the dye streakline image shown in figure 3(b). In figures 10(c) and 10(d) the piston has stopped and the piston vortex appears to be convecting toward the axis of symmetry and stretching along this axis toward the stagnation point of the primary vortex. This result also agrees well with the flow visualization that showed a bulge produced by the ingestion of the piston

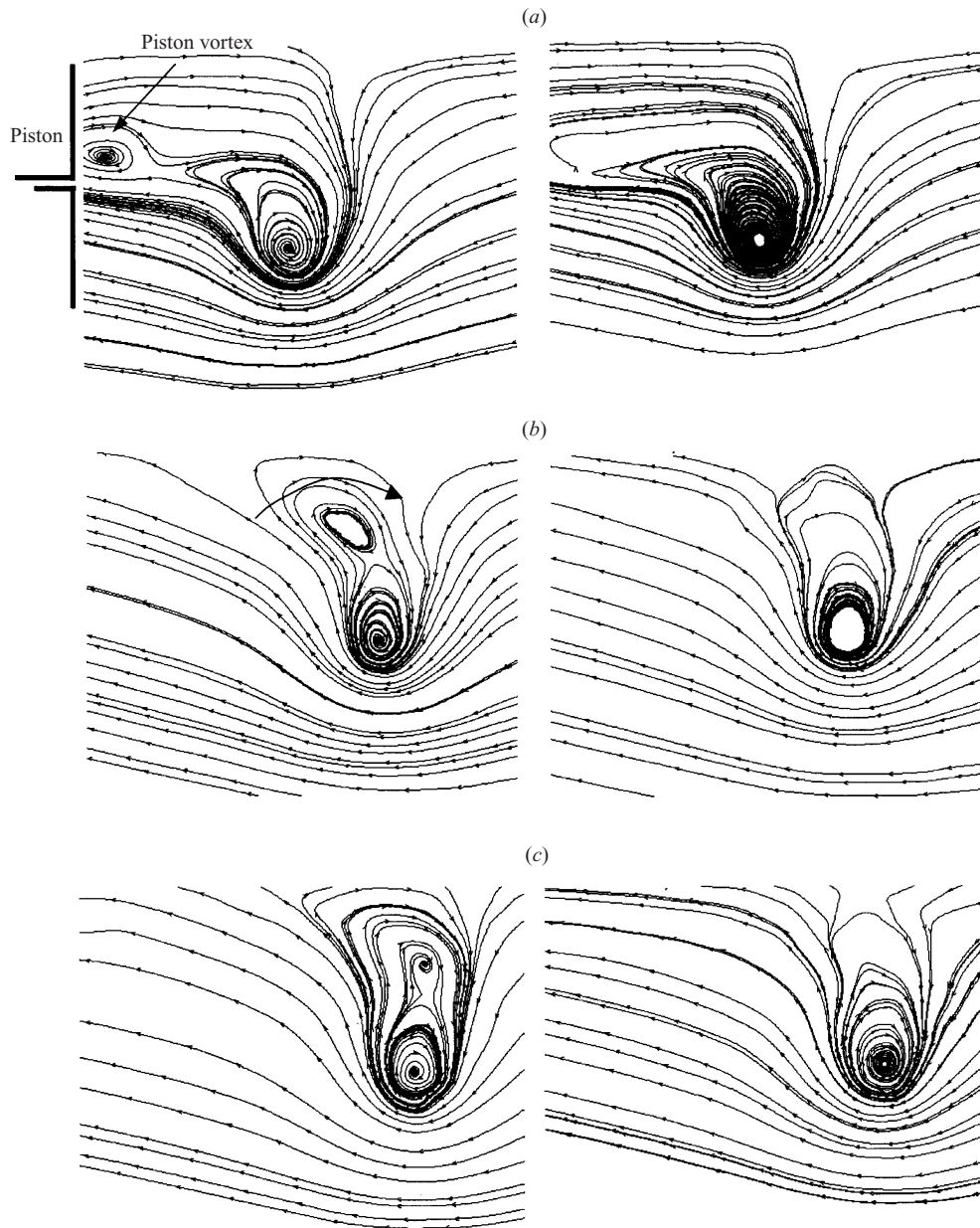


FIGURE 9. Streamline patterns for $Re_T = 6530$, $L/D = 2$, left column $S/D = 0$, right column $S/D = 2$. (a) $t^* = 2.17$, (b) $t^* = 2.77$, (c) $t^* = 3.37$.

vortex, figure 2(b). These results also appear similar to that of Fabris & Liepmann (1997), who examined the late stages of ring development and who also comment that although there may be some cancellation of the vorticity from the shear layers across the axis of the ring, a significant amount of vorticity is advected through the centre of the ring and collects in the region of the forward stagnation point, resulting in a more complex vorticity distribution than may otherwise have been expected. The peak level of the non-dimensional vorticity in the primary vortex is $\omega \sim 50$ and the

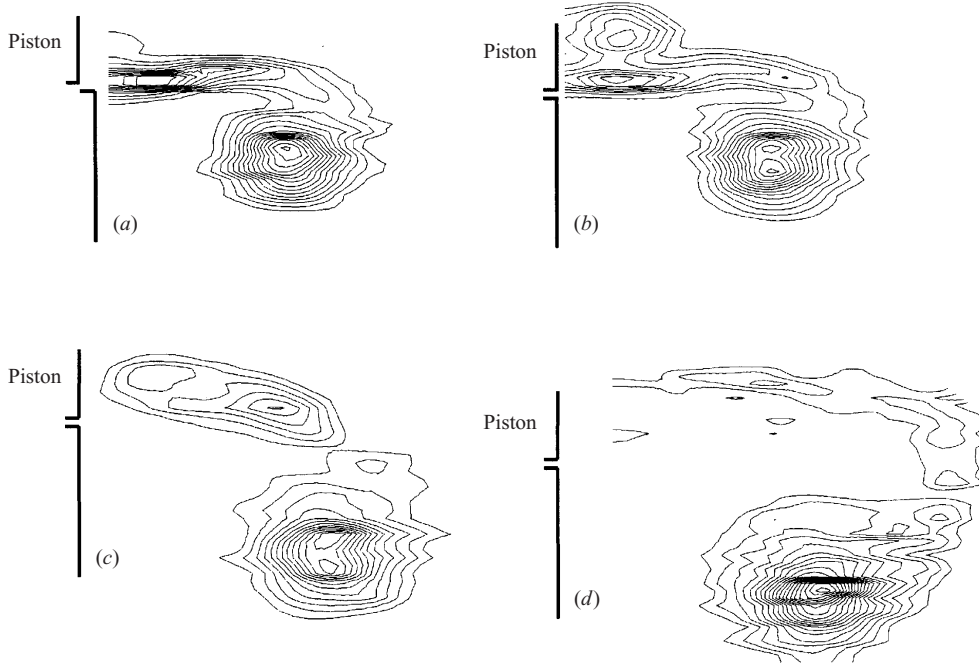


FIGURE 10. Vorticity fields for $Re_\tau = 6530$, $L/D = 2$, $S/D = 0$: (a) $t^* = 1.9$, (b) $t^* = 2.17$, (c) $t^* = 2.77$, (d) $t^* = 4.0$.

level in the piston vortex is $\omega \sim 13$, which agrees well with the results of Weigand & Gharib (1997) and Allen & Chong (2000). The vorticity distributions do not reveal any significant vorticity deposition into the wake.

Quantities of interest to describe the behaviour of vortex rings are the strength $\Gamma = \iint \Omega(r, \theta) dA$ and impulse $I = \rho\pi \iint \Omega(r, \theta) r^2 dA$. These quantities can be found by evaluating an area integral over the vorticity fields. Figures 11(a) and 11(b) show Γ/ν and $I/(\rho\pi D^2/4U_0)$ versus t^* for the case where the piston finishes flush with the wall, and when it finishes $2D$ inside the tube for $Re_\tau = 6530$. They show that when the piston finishes flush with the wall the ring has a larger impulse and strength. This corroborates the conjecture in §5.2 that the increased convection speed for $S/D = 0$ was related to the higher circulation of the primary ring. The size of the difference in ring strength, of the order 6%, is similar to the difference in convection speed. This difference in strength and impulse is most clearly illustrated in figure 12 which shows the vorticity distributions at the instant the piston motion has ceased for $S/D = 0$ and $S/D = 2$. The larger integral, and hence strength and impulse, for the $S/D = 0$ case is clearly due to the presence of the piston vortex that can be seen being ejected in front of the piston. The results for ring strength, for $L/D = 2$, are of the order $\pm 5\%$ of that shown in Didden (1979, figure 15). It should also be noted that the area integral used for the calculation of impulse and strength for the case where the piston ceases its motion inside the tube does not incorporate the stopping vortex and hence the impulse and strength calculated are for the primary ring. With our two stopping configurations, the small variation in impulse and strength is clearly explained as a result of the ingestion of the piston vortex, rather than an effect of the stopping vortex.

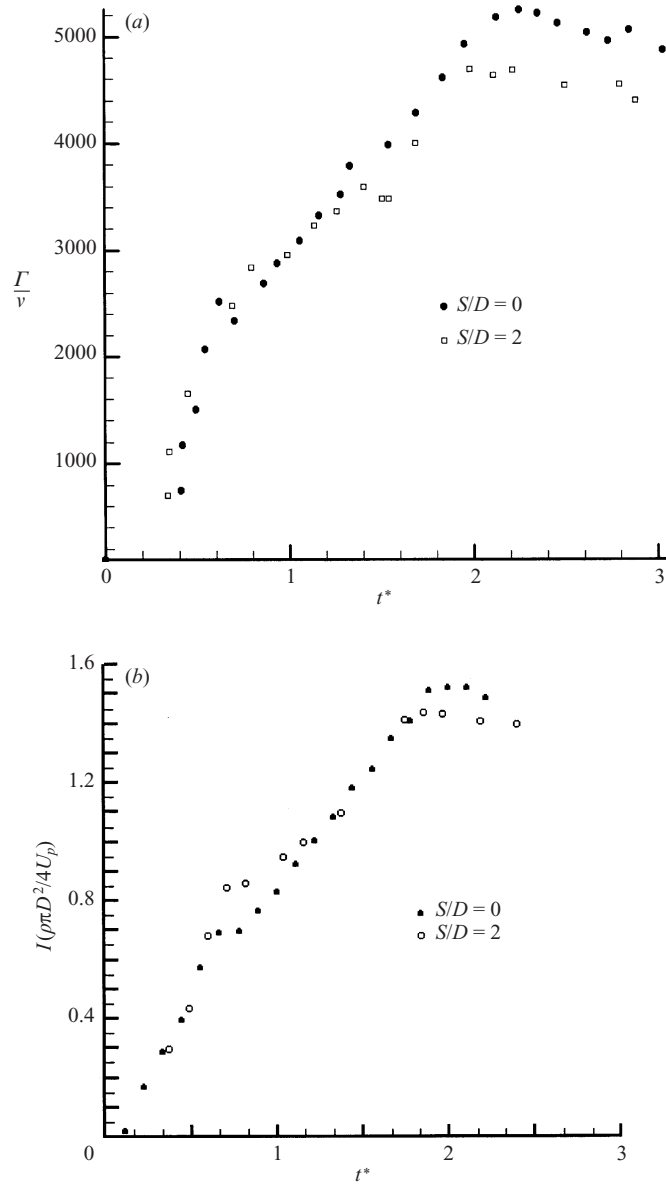


FIGURE 11. (a) Γ/v and (b) $I/(\rho\pi D^2/4U_p)$ versus t^* for $Re_r = 6530$ and $S/D = 0, 2$, $L/D = 2$.

6. Development of azimuthal instabilities on the piston vortex

Glezer (1988) noted the presence of an azimuthal core instability on the primary ring that consisted of vortex tubes, alternating in sense, wrapped around the main core of the vortex that resembled the braids that appear in shear layers, e.g. Bernal & Roshko (1986). He also commented that these tubes are responsible for the entrainment and detrainment of fluid to and from the vortex ring and suggested that these tubes had their origin on the connecting shear layer between the vortex core and the orifice and that their presence accelerates the transition to turbulence.

To determine the origin of these instabilities on the ring observed by Glezer (1988) and commented on by Auerbach (1991), a global visualization technique was

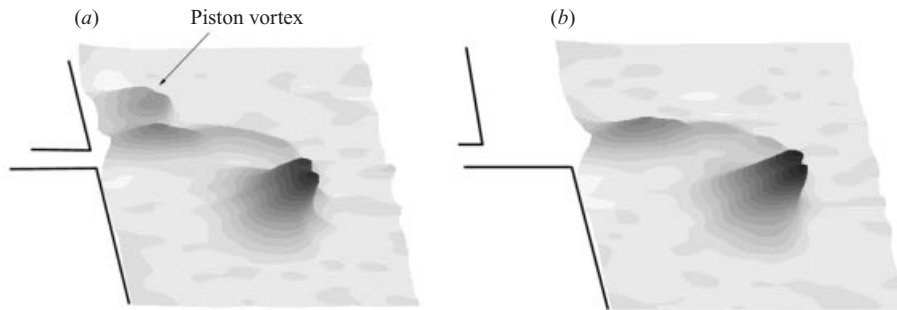


FIGURE 12. Variation in vorticity distribution at $Re_T = 6530$, $t^* = 2.17$ for (a) $S/D = 0$, (b) $S/D = 2$.

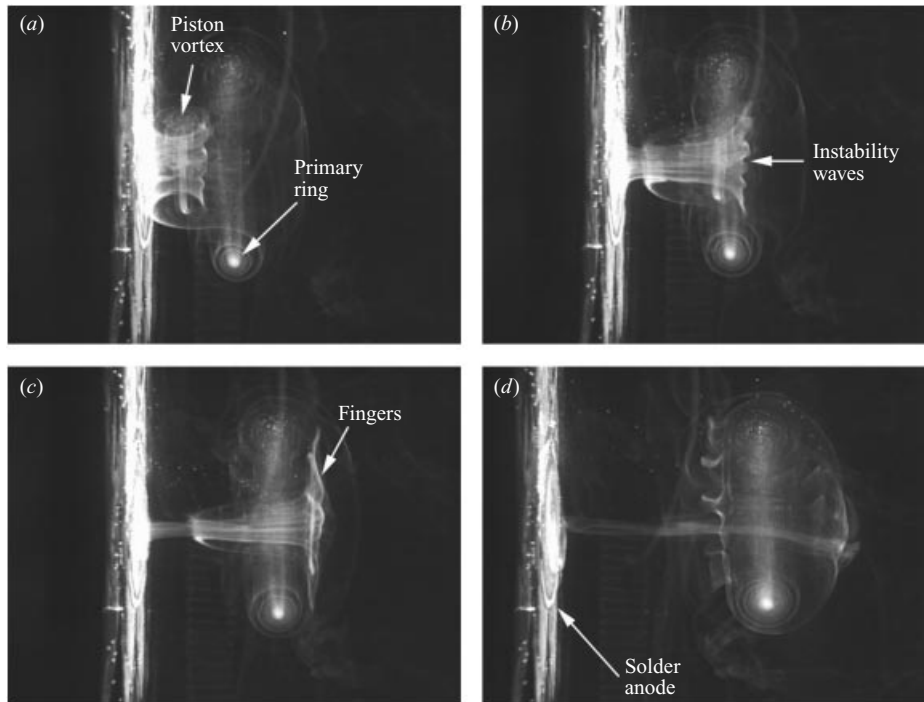


FIGURE 13. Precipitate flow visualization images for $Re_T = 6530$, $L/D = 2$: (a) $t^* = 2.17$, (b) $t^* = 2.65$, (c) $t^* = 3.3$, (d) $t^* = 5.8$.

employed. A metallic precipitate was created at the edge of the orifice using a loop of tinned solder. The thickness of the solder loop was of order 0.5 mm and was located on the wall at a distance of 1 mm from the orifice so as to not disturb the vortex ring generation process. The solder, acting as the anode, was connected to an 80 V power source. The primary benefit of this method is that white light could be used to provide a three-dimensional image of the ring development. The Schmidt number of the precipitate is of order 1000, see Taneda (1977) for details. Figure 13 shows a sequence of results for the case when piston motion finishes flush with the wall. Figure 13(a) shows the piston vortex and primary ring at the instant the piston motion has stopped. Wave-like structures are seen on the outer turn of the piston vortex. No waves are apparent on the core of the piston vortex, or on the primary ring.

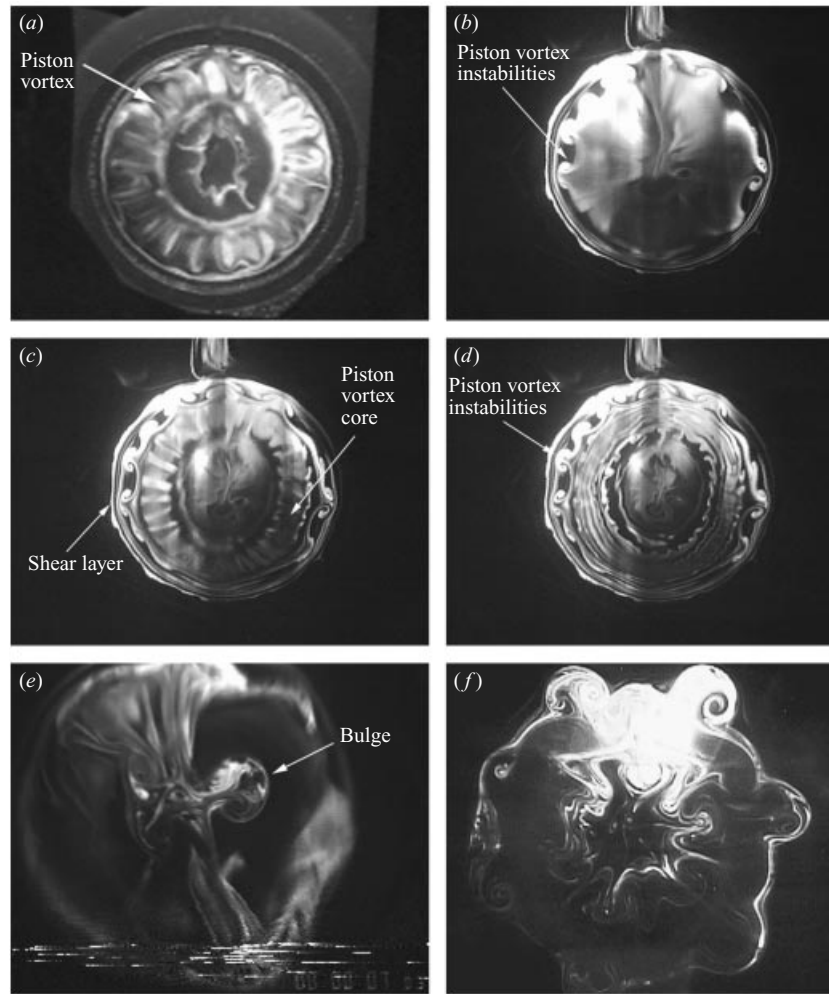


FIGURE 14. Laser cross-sections for $Re_r = 13\,390$ and $L/D = 4$, $S/D = 0$: (a) $Z/D = -1.64$, $t^* = 3.32$; (b) $Z/D = 0.35$, $t^* = 4.18$; (c) $Z/D = 0.35$, $t^* = 4.24$; (d) $Z/D = 0.35$, $t^* = 4.32$; (e) $Z/D = 3.15$, $t^* = 6.85$, (f) $Z/D = 6$, $t^* = 9.0$.

These wave-like structures persist throughout the entrainment process. In figure 13(b) the waves on the piston vortex can be seen passing through the primary ring. As the piston vortex reaches the stagnation point of the main ring, these structures can be seen wrapping rapidly around the outside of the primary vortex in a finger-like fashion, figure 13(c). In figure 13(d), the tips of the structures can be seen in the wake of the ring as a series of jellyfish-like tentacles. To gain a further insight into the nature of these structures, their time evolution and wavelength, laser cross-sections were taken through planes perpendicular to the direction of propagation of the ring. Results of flow visualization experiments using fluorescent dye are shown in figure 14 for a range of Z/D locations from the wall, where Z is the streamwise distance from the orifice exit.

Figure 14(a) shows a cross-section of the piston vortex at the location $Z/D = -1.64$, at $t^* = 3.32$. This represents a cross-section inside the tube, before the piston vortex has been ejected. Periodic structures can be seen distributed around the azimuth on

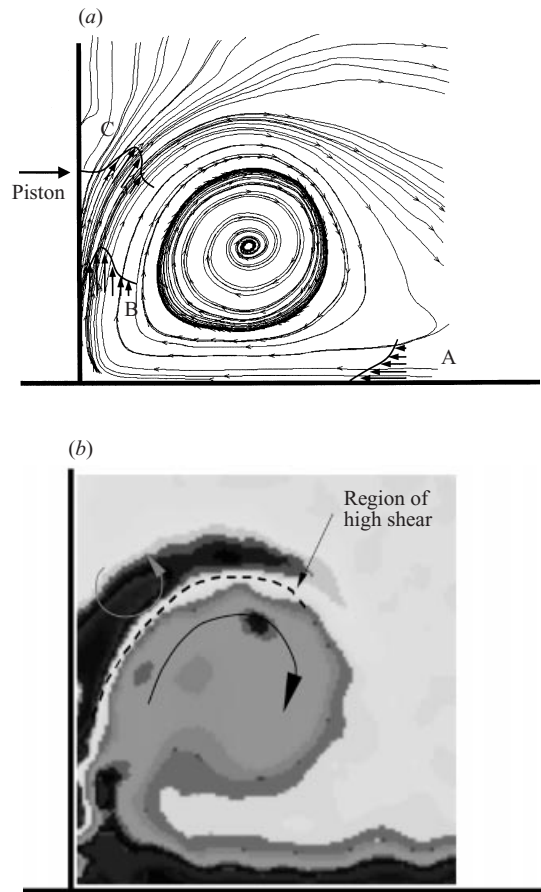


FIGURE 15. Streamline pattern (a) and vorticity field (b) in the piston/cylinder corner region from Allen & Chong (2000).

the piston vortex, indicating that the source of the instability is not related to the presence of the primary ring. Figures 14(b) and 14(c) show cross-sections at a location $Z/D = 0.35$, downstream of orifice. The cross-sections marked A and B in figure 2(c) mark the approximate location where these cross-sections are taken relative to the evolution of the piston vortex. In the images in figures 14(b) to 14(d) the primary ring has already passed through the laser sheet. The outer circle of dye represents the shear layer that connects the primary ring to the orifice exit. Figure 14(b) shows the head of the piston vortex as it starts to enter the illumination plane. Instabilities on the outer edge of the piston vortex can be clearly seen in figure 14(c), as can the connecting filaments running across the top of the piston vortex. Figure 14(d) shows the same cross-section through the core of the piston vortex a short time later. The connecting filaments are no longer visible, but instabilities on the outer edge of the piston vortex can be clearly seen, along with some waviness on the inner turns of the piston vortex. The visualizations indicate the presence of vorticity filaments aligned in a plane perpendicular to the azimuthal direction. This represents a significant reorientation of the vorticity on the piston vortex. The number of azimuthal structures is of order twelve. Varying Re_F did not appear to significantly alter the number of waves that were forming but did effect how rapidly they developed. The instability does not seem to have its origin on the piston vortex core. Figure 14(e) shows a cross-section through

the vortex at a location $Z/D = 3.15$, at $t^* = 6.85$. The cross-section shown as C in figure 2(c) represents the approximate location of this point. This image shows the ‘bulge’ identified in earlier visualizations. The presence of streamwise piston-generated fingers can be seen clustered in the stagnation point region. The stretching of two of these structures around the outer periphery of the primary vortex is also evident. Figure 14(f) clearly shows the presence of these vortical fingers on the periphery of the primary vortex.

7. Instability mechanism

It appears from the flow visualization images that the instability has its source on the outer turn of the piston vortex. In order to construct a physical mechanism for the generation of these structures one must consider how the piston vortex is being generated. Figure 15 shows an example of the streamline pattern and vorticity field in the region of the junction of the piston/cylinder wall from Allen & Chong (2000). This is a cross-section of one side of the piston vortex relative to an observer moving with the piston.

The process of formation of this structure is that when the piston is set in motion, a boundary layer forms on the cylinder wall, shown with the velocity profile at point A. The boundary layer is turned through 90° at the piston junction resulting in the production of significant secondary vorticity on the piston face and resulting in a ‘wall jet’ type velocity profile, shown at point B. The boundary layer then diverges rapidly away from the piston surface, shown by the velocity profile at point C and rolls up into a vortical structure, described in this paper as the ‘piston vortex’. The wall jet nature of the velocity profile on the piston face indicates two regions of opposite signed vorticity, and diverging flow at point C is subject to high curvature. These two layers of opposite signed vorticity can be clearly seen in figure 15(b).

A wall jet subject to concave curvature is unstable due to the presence of centrifugal forces, see Floryan & Saric (1984). It is in the inner flow, the section of the flow between the wall and the point of maximum velocity, that the instability will first develop in a wall jet subject to concave curvature. The control parameter for the stability of wall jets subject to concave curvature is the Görtler number,

$$G_0 = U_\infty \delta / \nu \times \sqrt{\delta / R},$$

where U_∞ is the maximum velocity of the wall jet, R is the radius of curvature and δ is the wall jet thickness. A criterion for the development of Görtler vortices in the wall jet with concave curvature is $G_0 > 1.0$. There is no critical wavenumber and the characteristics of the vortices are determined by the disturbance growth process. Experiments to determine the natural wavelength of Görtler vortices have been found to be extremely sensitive to the properties of the apparatus and its flow field. Bippes (1978) recorded the wavelength of the Görtler vortex as being that of the highest amplification rate from linear theory, and once the wavelength is established it is preserved downstream. Following Floryan (1987) we can consider the dimensionless wavelength parameter

$$A = F^{1/3} \lambda^{1/3} \nu^{-1} (\lambda / R)^{1/2},$$

where F is the dimensional ‘flux of external momentum flux’, see Glauert (1956). A is constant in the flow direction in order to follow a vortex of constant dimensional wavelength λ . The curve of maximum growth from the linear stability analysis of Floryan (1987) shows a variation of A from 48 to 85. From experiments with the piston moving at 66 mm s^{-1} an estimate of $U_\infty \approx 30 \text{ mm s}^{-1}$ at a location 2.5 mm

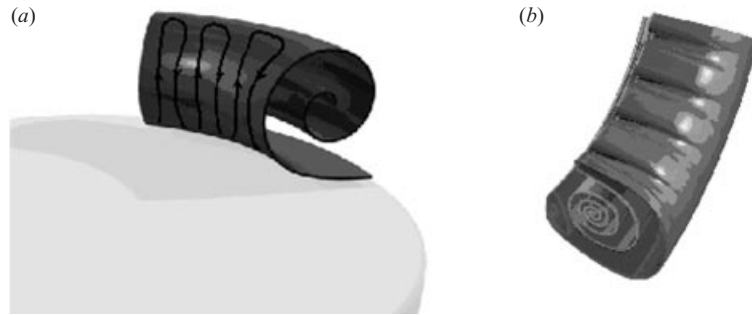


FIGURE 16. (a) Schematic of instability development on the piston and (b) ingestion of the piston vortex and instability during the steady translation phase.

above the piston face is obtained. An approximation for the wall jet thickness is $\delta \approx 8$ mm and a radius of curvature of $R \approx 12$ mm. This results in a Görtler number, $G_0 = U_\infty \delta / \nu \sqrt{\delta/R}$, in excess of 100 and hence instabilities should be present. Using a crude approximation for the velocity profile an estimate can be made of $F \approx 1.63 \times 10^5 \text{ mm}^5 \text{ s}^{-3}$ which results in an approximation of $\lambda \approx 1.4$ mm to 8 mm. The wavelength of the structures in figure 14(a) is of order 8 mm and hence it would appear that the instability is of centrifugal form.

Once the region of secondary vorticity plume and neighbouring piston vortex has been perturbed it is anticipated that the nonlinear growth of the instability follows a similar nonlinear growth mechanism to that outlined by Lasheras, Cho & Maxworthy (1986). They presented a physical model for the generation of the streamwise structures via nonlinear vortex stretching and tilting in the highly strained braid region of a shear layer. A similar region of high shear exists on the outer turn of the piston vortex, as illustrated in figure 15(b). This stretching process is illustrated in figure 16(a). This instability is rolled/entrained into the piston vortex as the structure develops in front of the advancing piston. When the piston vortex is ejected and ingested into the primary ring the instabilities produce the fingers seen in figure 13(c) and the filaments in figure 14(a). This development process is shown in schematic form in figure 16(b), where the rolled-up vortex sheet that constitutes the primary ring is shown as being connected to the piston vortex and the instability is superimposed on the vortex sheet that is wrapped around the primary ring.

8. Transition to turbulence

If Re_D exceeds 600, then as the vortex convects away from the tube, azimuthal waves associated with the Tsai–Widnall instability begin to appear. This leads to an eventual breakdown to turbulence. These waves develop because the strain field at a perturbed point on the vortex ring is sufficient to overcome the self-induced azimuthal core rotation. The most unstable waves grow at an angle of the order 45° to the axis of symmetry, without precessing about the ring core. The image in figure 17(a) shows the formation of these waves for $Re_r = 6530$ at $Z/D \sim 8$. Saffman (1978) noted that although the mechanism for the generation of waves on the ring is an inviscid one, the number of waves that appear on a vortex ring is a function of the shape of the vorticity distribution within the ring, and hence a function of Reynolds number. The calculations of Saffman (1978) agree well with the experiments of Liess & Didden (1976), who found an experimental variation of the number of waves forming on

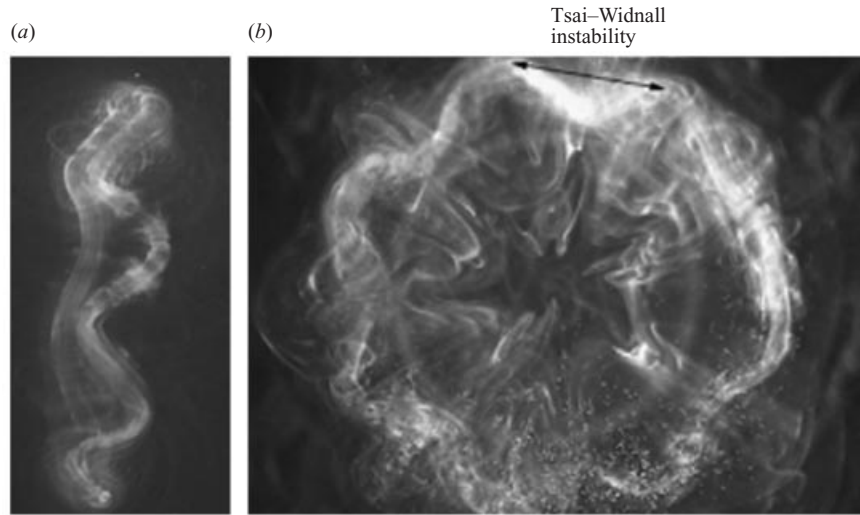


FIGURE 17. Development of Tsai-Widnall instabilities $Re_\Gamma = 6530$, $t^* = 17$, $S/D = 0$, $L/D = 2$.

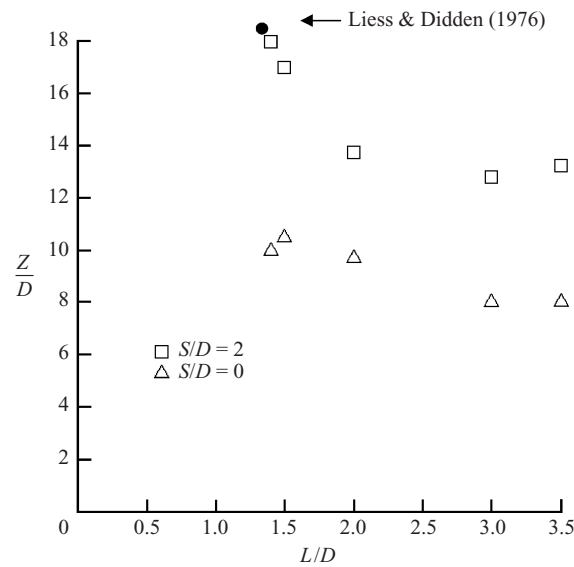


FIGURE 18. Distance travelled from tube exit to turbulence breakdown for $Re_D = 3120$.

the ring from 4 to 11 as Re_D was varied from 2000 to 10 000 with $L/D = 1.4$. For $Re_\Gamma = 6530$ the number of waves is of the order of eight. This is in good agreement with the results of Liess & Didden (1976). The image in figure 17(b), which shows the classical Tsai-Widnall instability just prior to vortex breakdown to turbulence, also shows evidence of filaments on the outer diameter. These structures had their origin on the piston vortex. In the current experiments it was found that the number of waves forming on the primary ring appears to be insensitive to whether the piston vortex is ingested or not for a given Re_Γ . The reason for the insensitivity is that the perturbation introduced by the ingestion of the piston vortex is small, relative to the change in strength required to produce a change in the wavenumber. The data of

Liess & Didden (1976) show that, in the Reynolds number range we are working in, a doubling of the vortex strength will increase the number of waves from 8 to 10.

The distance to transition to turbulence, as determined from flow visualization experiments, is plotted in figure 18. The results show that there is an effect of the piston vortex on the transition distance. The amplification rate of the Tsai–Widnall instability appears greater when the piston vortex is ingested. For $L/D > 1.5$ the distance travelled by the ring that has not ingested the piston vortex is of order 40% greater than the case where it has. In terms of the time to transition there is as much as a 50% difference as when the piston vortex is ingested the ring moves faster. The linear, uniform core, inviscid analysis of Widnall, Bliss & Tsai (1974) suggests that the amplification rate of the instability is proportional to the ring strength. Given the fact that the overall differences in ring strengths are of order 5% and that the ring diameters are virtually identical, the linear analysis does not provide a good reason for the large difference in transition distance. The causes are more likely to lie with the effect of the piston vortex in producing a non-uniform vorticity distribution within the core which results in a strong nonlinear effect on the growth rate of the Tsai–Widnall disturbance. Comparison with the data of Liess & Didden (1976) was good for the case of $L/D = 1.4$ and the piston stopping inside the tube. The errors in measurements of the distance to transition are of order $\pm 4\%$.

9. Conclusions

The simple formation geometry of a piston finishing flush with a normal wall to produce a vortex is shown to introduce an interesting flow complexity. While eliminating the stopping vortex, a piston vortex is ejected and entrained into the primary ring. L/D in this experiment was varied from 1 to 4, where L is the stroke of the piston. In all the cases when the piston was stopped flush with the wall, ingestion occurred. This ingestion appears to have a measurable effect on the speed of the primary ring and measurements confirm that ingestion of the piston vortex provides an added impulse to the ring. The absorption of the piston vortex has also been measured in terms of its effect on the unsteady streamline field and vorticity distribution. The piston vortex appears to be entrained toward the forward stagnation point on the ring, where it is rapidly strained and convected around the periphery of the primary vortex core. There is evidence of a centrifugal instability on the piston vortex which has the effect of generating vorticity filaments in the plane perpendicular to the azimuthal direction. These instabilities are entrained into the main ring and could be the origin of the instabilities observed by Glezer (1988). It appears that the piston vortex, although not affecting the basic mechanism for transition, has a secondary effect on transition in that it reduces the distance the ring convects before transition occurs because it amplifies the growth rate of the Tsai–Widnall instability. This would also suggest that the transition map proposed by Glezer (1988) is geometry specific.

The authors would like to acknowledge the support of Professor A. J. Smits and the NSF, grant number CTS-9706902.

REFERENCES

- ALLEN, J. J., AUIVITY, B. & SMITS, A. J. 2000 Interaction of a vortex ring with a piston vortex. *9th Intl Symposium on Flow Visualization, Edinburgh, August 22–25* (ed. I. Grant & G. M. Carlomagno). ISBN 0 9533991 17.
- ALLEN, J. J. & CHONG, M. S. 2000 Vortex formation in front of a piston moving through a cylinder. *J. Fluid Mech.* **416**, 1–28.

- ALLEN, J. J. & SMITS, A. J. 2001 Energy harvesting eel. *J. Fluids Struct.* **15**, 629–640.
- AUERBACH, D. 1987 Experiments on the trajectory and circulation of the starting vortex. *J. Fluid Mech.* **183**, 185–198.
- AUERBACH, D. 1991 Stirring properties of vortex rings. *Phys. Fluids A* **3**, 1351–1355.
- BERNAL, L. P. & ROSHKO, A. 1986 Streamwise vortex structure in plane mixing layers. *J. Fluid Mech.* **170**, 499–526.
- BIPPES, H. 1978 Experimental study of the laminar–turbulent transition of a concave wall in parallel flow. *NASA TM* 75243.
- CATER, J., SORIA, J. & LIM, T. T. 1998 Vortex ring formation at an orifice. In *Advances in Turbulence VII* (ed. U. Frisch), pp. 15–18. Kluwer.
- DIDDEN, N. 1979 On the formation of vortex rings rolling-up and production of circulation. *Z. Angew. Math. Phys.* **30**, 101–116.
- FABRIS, D. & LIEPMANN, D. 1997 Vortex ring structure at late stages of formation. *Phys. Fluids* **9**, 2801–2803.
- FLORYAN, J. M. 1987 Görtler Instability of wall jets. *AIAA J.* **27**, 112–115.
- FLORYAN, J. M. & SARIC, W. S. 1984 Wavelength selection and growth of Görtler vortices. *AIAA J.* **22**, 1529–1538.
- GHARIB, M., RAMBOD, E. & SHARIF, K. 1998 A universal time scale for vortex ring formation. *J. Fluid Mech.* **360**, 121–140.
- GLAUERT, M. B. 1956 The wall jet. *J. Fluid Mech.* **1**, 625–643.
- GLEZER, A. 1988 The formation of vortex rings. *Phys. Fluids* **32**, 3532–3542.
- GLEZER, A. & COLES, D. 1990 An experimental study of a turbulent vortex ring. *J. Fluid Mech.* **211**, 243–283.
- HEEG, R. S. & RILEY, N. 1997 Simulations of the formation of an axisymmetric vortex ring. *J. Fluid Mech.* **339**, 199–211.
- HUGHES, M. D. & GERRARD, J. H. 1971 The stability of unsteady axisymmetric incompressible pipe flow close to a piston. Part 2. Experimental investigation and comparison with computation. *J. Fluid Mech.* **50**, 645–655.
- JAMES, S. & MADNIA, C. K. 1996 Direct numerical simulation of a laminar vortex ring. *Phys. Fluids* **8**, 2400–2414.
- KADEN, H. 1931 Aufwicklung einer unstablen Unstetigkeitsfläche. *Ing. Arch.* **2**, 140–168.
- LASHERAS, L., CHO, J. S. & MAXWORTHY, T. 1986 On the origin and evolution of streamwise vortical structures in a plane, free shear layer. *J. Fluid Mech.* **172**, 231–258.
- LISS, L. & DIDDEN, N. 1976 Experimente zum einfluss der Anfangsbedingungen auf die Instabilität von Ringwirbeln. *Z. Angew. Math. Mech.* **56**, T206–T208.
- LIM, T. T. 1997 On the role of Kelvin-Helmholtz like instability in the formation of turbulent vortex rings. *Fluid Dyn. Res.* **21**, 47–56.
- LIM, T. T. & NICKELS, T. B. 1995 Vortex rings. In *Vortices in Fluid Flows* (ed. S. I. Green). Kluwer.
- MAXWORTHY, T. 1974 Turbulent vortex rings. *J. Fluid Mech.* **64**, 227–240.
- MAXWORTHY, T. 1977 Some experimental studies of vortex rings. *J. Fluid Mech.* **81**, 465–495.
- MOHSENI, K. & GHARIB, M. 1998 A model for universal time scale of vortex ring formation. *Phys. Fluids* **10**, 2436–2438.
- NITSCHKE, M. 1996 Scaling properties of vortex ring formation at a circular tube opening. *Phys. Fluids* **8**, 1849–1855.
- NITSCHKE, M. 2001 Self-similar shedding of vortex rings. *J. Fluid Mech.* **435**, 397–407.
- NITSCHKE, M. & KRASNY, R. 1994 A numerical study of vortex ring formation at the edge of a circular tube. *J. Fluid Mech.* **276**, 139–161.
- POZRIKIDIS, C. 1986 The nonlinear instability of Hill's vortex. *J. Fluid Mech.* **168**, 337–367.
- PULLIN, D. I. 1978 The large-scale structure of unsteady self-similar rolled-up vortex sheets. *J. Fluid Mech.* **88**, 401–430.
- PULLIN, D. I. & PERRY, A. E. 1980 Some flow visualization experiments on the starting vortex. *J. Fluid Mech.* **97**, 239–255.
- ROM-KEDAR, V., LEONARD, A. & WIGGINS, S. 1990 An analytical study of the transport, mixing and chaos in an unsteady vortical flow. *J. Fluid Mech.* **214**, 347–394.
- ROSENFELD, M., RAMBOD, E. & GHARIB, M. 1998 Circulation and formation number of laminar vortex rings. *J. Fluid Mech.* **376**, 297–318.

- SAFFMAN, P. G. 1978 The number of waves on unstable vortex rings. *J. Fluid Mech.* **84**, 625–639.
- SHARIFF, K. & LEONARD, A. 1992 Vortex rings. *Annu. Rev. Fluid Mech.* **24**, 235–279.
- SHEFFIELD, J. S. 1977 Trajectories of an ideal vortex pair near an orifice. *Phys. Fluids* **20**, 543–545.
- SPEDDING, G. & RIGNOT, E. 1993 Performance analysis and application of grid interpolation techniques for fluid flows. *Exps. Fluids* **10**, 417–430.
- TABACZYNSKI, R. J., HOULT, D. P. & KECK, J. C. 1970 High Reynolds number flow in a moving corner. *J. Fluid Mech.* **42**, 249–255.
- TANEDA, S. 1977 Visual study of unsteady separated flows around bodies. *Prog. Aerospace Sci.* **17**, 287–348.
- TAYLOR, G. I. 1960 *Aeronautics and Aeromechanics*. Pergamon.
- WEIGAND, A., GHARIB, M. 1997 On the evolution of laminar vortex rings. *Exps. Fluids* **22**, 447–457.
- WIDNALL, S. E., BLISS, D. B. & TSAI, C. 1974 The instability of short waves on a vortex ring. *J. Fluid Mech.* **66**, 35–47.
- WIDNALL, S. E. & TSAI, C.-Y. 1977 The instability of the thin vortex ring of constant vorticity. *Phil. Trans. R. Soc. Lond. A* **287**, 273–305.
- YAMADA, H. & MATSUI, T. 1978 Preliminary study of mutual slip-through of a pair of vortices. *Phys. Fluids* **21**, 292.